Special Section: Vadose Zone Modeling
Vadose Zone Journal

Modeling Coupled Hydrologic and Chemical Processes: Long-Term Uranium Transport following Phosphorus Fertilization

D. Jacques,* J. Šimůnek, D. Mallants, and M.Th. van Genuchten

Coupling physical and geochemical processes within one integrated numerical simulator provides a process-based tool for investigating the mobility of contaminants as affected by changing hydrologic regimes and geochemical conditions. We review interactions between physical and biogeochemical processes in the vadose zone, and then present a case study demonstrating these complex interactions. A hypothetical application is presented of the HP1 multicomponent transport simulator to predict the transport of two major elements (Ca and P) and one trace element (U) applied annually for 200 yr to a field soil in the form of an inorganic P fertilizer. Interactions of Ca, P, and U with the solid phase are described using cation exchange and surface complexation reactions. Simulations assuming steady-state or transient flow conditions were analyzed in terms of temporal variations of the linear distribution coefficient, K_d, which depends strongly on pH and the composition of the aqueous phase. If the composition of the aqueous phase is constant, adsorption of Ca and U increases with increasing pH. Due to the annual addition of Ca, P, and U, and competition between P and U for sorption sites, the K_d of these elements decreased with time near the soil surface. Deeper in the soil, the K_d of U followed the pH increase because of a lack of competition from P. Because of the combined effects of changing hydrologic and geochemical conditions, the Ca and U distribution coefficients and solute fluxes during the transient simulation exhibited large short-time variations of up to three orders of magnitude.

FIELD SOILS are complex three-dimensional heterogeneous systems involving the transport, redistribution, and transformation of multiple components in different phases under nonisothermal conditions. The various transformations are to a large extent initiated, directed, and catalyzed by (micro)biological agents. The transport of components is not limited to only chemical elements such as major cations and anions, heavy metals, radionuclides, or organic pollutants, but often also involves organic and inorganic colloids and microorganisms. Vegetation furthermore interacts with the soil, mainly through its roots, which extract water and nutrients from the soil. Roots at the same time release various organic ligands to mobilize nutrients and alter geochemical conditions near the root–soil interface (e.g., Seuntjens et al., 2005; Calba et al., 2004; Geelhoed et al., 1999).

An integrated approach is necessary for understanding and unraveling the complex interplay of different soil processes. Integration of all pertinent processes into a numerical transport modeling tool is indispensable for evaluating the various coupled effects involved (e.g., Mayer et al., 2002; Metz et al., 2002; Davis et al., 2004b; Lichtner et al., 2004; Appelo and Postma, 2005; Nützmann et al., 2005; Nuclear Regulatory Commission, 2006; Carrillo-González et al., 2006). Steefel et al. (2005) briefly discussed some historical steps in the development of such tools. Many reactive transport codes of different levels of complexity have been developed during the last few decades for saturated porous media (e.g., van der Lee and De Windt, 2001). More recently, similar codes started to consider also flow and transport in the unsaturated zone. Examples are 3DHYDROGEOCHEM (Yeh and Cheng, 1999), CORE^{2D} (Samper et al., 2000), MIN3P (Mayer et al., 2002), Pollutrans (Kuechler and Noack, 2002), UNSATCHEM-2D (Šimůnek and Suarez, 1994), RETRASO (Saaltink et al., 2004), HYDRUS-1D (Šimůnek et al., 2005), and HP1 (Jacques et al., 2006b). Thus far, most applications of these multicomponent transport models to both saturated and unsaturated conditions have been limited to steady-state flow scenarios.

Transient flow in soils can substantially affect geochemical conditions for both equilibrium and kinetic reactions. Experimental evidence shows that alternations in infiltration (due to precipitation and irrigation) and evaporation periods, or changes in temperature, can strongly influence geochemical conditions near the soil surface. Such effects have been demonstrated during experimental cycles in laboratory setups (e.g., Öztürk and Özkan, 2004), seasonal variations in the field (e.g., Berner et al., 1998), and for artificial recharge of groundwa-

D. Jacques and D. Mallants, Performance Assessments Unit, Belgian Nuclear Research Centre (SCK·CEN), Boeretang 200, B-2400 Mol, Belgium; J. Šimůnek, Dep. of Environmental Sciences, Univ. of California, Riverside, CA 92521; M.Th. van Genuchten, USDA-ARS, U.S. Salinity Lab., 450 W. Big Spring Rd., Riverside, CA 92507. Received 27 Apr. 2007. *Corresponding author (djacques@sckcen.be).

Vadose Zone J. 7:698–711
doi:10.2136/vzj2007.0084

ter (Greskowiak et al., 2005). The interaction of discharging groundwater and shallow groundwater dynamics with temporal variations in atmospheric conditions also affects the soil water composition (e.g., de Mars et al., 1997; de Mars and Garritsen, 1997; Joris, 2005). Slattery and Ronnfeldt (1992) showed that seasonal variations in pH were partly related to ionic strength. Gonçalves et al. (2006) reported an experimental study to quantify salinization and alkalization risks in lysimeters exposed to natural atmospheric conditions (rainfall and evapotranspiration) and manually irrigated with waters of different quality. Overall salinity and Na concentrations changed significantly during the year. Sodium concentrations near the soil surface peaked during dry periods after irrigation events, but subsequently decreased again to initial values during rainfall periods. The experimental data were successfully simulated using HYDRUS-1D, which couples an ion chemistry module with a water flow and solute transport model.

A similar behavior for Na was found by Jacques et al. (2008) in a hypothetical simulation of the 30-yr migration of heavy metals under atmospheric conditions. During periods with a precipitation deficit (i.e., when potential evaporation is larger than precipitation), the pH near the soil decreased at the same time as the water content. The pH decrease was caused by increased ionic strength (i.e., higher concentrations) and the accumulation of anions such as Cl^- near the soil surface due to upward flow. In addition, the total amount of Cd in soil water also increased during the summer due to (i) increased competition of monovalent cations for the exchange sites (especially with Na, which is a more mobile element than K and thus accumulates near the soil surface during upward flow), and (ii) increased aqueous complexation of Cd and Cl.

Water content variations also influence the rate of kinetic reactions due to their effects on the wetted reactive area. The reactive surface area is a critical parameter affecting the rate of mineral dissolution. It is not straightforward to link reactive surface area to experimentally (e.g., BET mineral surface areas) or geometrically determined values. Brantley (2003) reported several reasons for this discrepancy: (i) the difference in reactivity of different surface sites (e.g., edge vs. basal plane sites for phyllosilicates); (ii) aging effects; (iii) the occurrence of deep etch cavities inducing transport-limited microenvironments for dissolution; and (iv) coatings of natural mineral surfaces with organic matter, Fe, Al, and Si. The critical parameter during transient unsaturated flow is the specific solid–water interfacial area, which varies as a function of the water content. In a theoretical study, Saripalli et al. (2006) showed that the interfacial area changed only slightly near saturation since the larger pores entail only a small percentage of the interfacial area, whereas a much stronger decrease in interfacial area occurs under dry conditions. Simulations for steady-state flow conditions involving different degrees of saturation illustrated that changing interfacial areas can have an important effect on solute fluxes. This effect of the degree of saturation was recently illustrated by Kuechler and Noack (2007) for pyrite–calcite dissolution during unsaturated flow. Only 5% of the batch-measured reactive surface area for pyrite was required to describe unsaturated column experiments at a degree of water saturation of 11%.

These examples illustrate the important effects transient water flow can have on multicomponent solute transport. Our main objective is to further demonstrate these types of interactions between transient flow and biochemical processes in soils. We first discuss various feedbacks between transient flow and other processes, and then present a hypothetical example involving the migration of several chemical species during a 200-yr time period. The governing vadose zone flow and chemical equations of the coupled HP1 multicomponent reactive transport code (Jacques and Šimůnek, 2005) are given next. Our focus is especially on nonlinear feedbacks between different processes relevant for soil systems. Then we show the important effects of the upper boundary condition (steady-state vs. transient flow) on the long-term migration of the main constituents (Ca and P) and a trace element (U) of an inorganic P fertilizer applied annually for 200 yr to a soil profile. The example demonstrates how transient water contents and fluxes affect soil pH, and hence the retention, bioavailability, and fluxes of various solute components.

Coupled Reactive Transport in the Vadose Zone

We will focus on interactions between various processes in the vadose zone by defining the governing equations (see also Steefel et al., 2005). Without attempting to be complete, selected feedbacks between processes important for unsaturated flow and transport problems will be discussed here. As a guide, we will outline the equations used in the HP1 multicomponent reactive transport simulator. This simulator couples two previously independent codes into one comprehensive tool. These are the HYDRUS-1D flow and transport model (Šimůnek et al., 2005) and the PHREEQC-2 biogeochemical model (Parkhurst and Appelo, 1999). More information about HP1, including the code itself, can be found at www.sckcen.be\hp1 (verified 18 Apr. 2008).

Processes and Reactions

Physical transport is described using the conservation equations for momentum, fluid mass, solute mass, and energy. Typically for soils and other porous materials, momentum conservation is described with the Darcy–Buckingham equation in combination with the conservation equation for water to yield the Richards equation as given by Eq. [1.1] in Table 1 (symbols are defined in the Appendix). We assume that the gas phase is continuous and at atmospheric pressure, which simplifies the description of fluid flow from a multiphase to a single-phase flow problem. To solve the Richards equation, the soil water content, θ [$L^3\ L^{-3}$], as a function of the soil water pressure head, h [L], and the unsaturated hydraulic conductivity, K [$L\ T^{-1}$], as a function of θ or h must be defined (e.g., Brooks and Corey, 1966; van Genuchten, 1980). The Richards equation describes uniform water flow in soils, but not any preferential or nonequilibrium flow. Alternative formulations for such conditions include various dual-porosity or dual-permeability models (see Šimůnek et al., 2003; Köhne et al., unpublished data, 2008; Šimůnek and van Genuchten, 2008).

When neglecting water vapor diffusion, the one-dimensional heat transport equation takes the form of Eq. [1.2] in Table 1. The volumetric heat capacity and thermal conductivity depend on various soil constituents (Campbell, 1985; Šimůnek et al., 2005), including the soil water content. Heat and water are also simultaneously transported as water vapor, which provides strong coupling between soil water and heat dynamics (e.g., Saito et al., 2006). The latter process is not included in HP1.

TABLE 1. Governing flow and transport equations, equilibrium geochemical mass-action equations, and examples of kinetic reaction equations used in HP1.

Process	Equation†	Equation no.
	Flow and Transport Equations	
Water flow (Richards equation)	$\frac{\partial \theta(h)}{\partial t} = \frac{\partial}{\partial x}\left[K(h)\left(\frac{\partial h}{\partial x} + \cos\alpha\right)\right] - S(h)$	[1.1]
Heat transport	$\frac{\partial C_{\mathrm{p}}(\theta)T}{\partial t} = \frac{\partial}{\partial x}\left[\lambda(\theta)\frac{\partial T}{\partial x}\right] - C_{\mathrm{w}}\frac{\partial qT}{\partial x} - C_{\mathrm{w}}ST$	[1.2]
Solute transport (advection-dispersion equation)	$\frac{\partial \theta C_j}{\partial t} = \frac{\partial}{\partial x}\left(\theta D^{w}\frac{\partial C_j}{\partial x}\right) - \frac{\partial qC_j}{\partial x} - SC_{\mathrm{r},j} + R_{\mathrm{o},j}$	[1.3]
	Chemical Equilibrium Reactions	
	Reaction Equation / Mass Action Law	
Aqueous speciation	$\sum_{j=1}^{N_{\mathrm{m}}}\nu_{ji}^{\mathrm{l}}A_j^{\mathrm{m}} = A_i \qquad K_i^{\mathrm{l}} = \gamma_i^{\mathrm{l}}c_i\prod_{j=1}^{N_{\mathrm{m}}}\left(\gamma_j^{\mathrm{m}}c_j^{\mathrm{m}}\right)^{-\nu_{ji}^{\mathrm{l}}}$	[1.4]
Ion exchange	$\sum_{j=1}^{N_{\mathrm{m}}}\nu_{ji_{\mathrm{e}}}^{\mathrm{e}}A_j^{\mathrm{m}} + \nu_{j_{\mathrm{e}}i_{\mathrm{e}}}^{\mathrm{e}}X_{j_{\mathrm{e}}}^{\mathrm{m}} = X_{i_{\mathrm{e}}} \qquad K_{i_{\mathrm{e}}}^{\mathrm{e}} = \gamma_{i_{\mathrm{e}}}^{\mathrm{e}}\beta_{i_{\mathrm{e}},j_{\mathrm{e}}}^{\mathrm{e}}\prod_{j=1}^{N_{\mathrm{m}}}\left(\gamma_j^{\mathrm{m}}c_j^{\mathrm{m}}\right)^{-\nu_{ji_{\mathrm{e}}}^{\mathrm{e}}}\left(\gamma_{j_{\mathrm{e}}}^{\mathrm{e}}\beta_{j_{\mathrm{e}},j_{\mathrm{e}}}^{\mathrm{e}}\right)^{-\nu_{j_{\mathrm{e}}i_{\mathrm{e}}}^{\mathrm{e}}}$	[1.5]
Surface complexation	$\sum_{j=1}^{N_{\mathrm{m}}}\nu_{ji_{\mathrm{s}}}^{\mathrm{s}}A_j^{\mathrm{m}} + \nu_{j_{\mathrm{s}}i_{\mathrm{s}}}^{\mathrm{s}}S_{j_{\mathrm{s}}}^{\mathrm{m}} = S_{i_{\mathrm{s}}} \qquad K_{i_{\mathrm{e}}}^{\mathrm{s,int}} = \left[\beta_{i_{\mathrm{s}},j_{\mathrm{s}}}^{\mathrm{s}}\prod_{j=1}^{N_{\mathrm{m}}}\left(\gamma_j^{\mathrm{m}}c_j^{\mathrm{m}}\right)^{-\nu_{ji_{\mathrm{s}}}^{\mathrm{e}}}\left(\beta_{j_{\mathrm{s}},j_{\mathrm{s}}}^{\mathrm{s}}\right)^{-\nu_{j_{\mathrm{s}}i_{\mathrm{s}}}^{\mathrm{s}}}\right]\exp\left(\frac{F\Psi_{j_{\mathrm{s}}}}{RT}\Delta z_{i_{\mathrm{s}}}\right)$	[1.6]
Mineral dissolution	$\sum_{j=1}^{N_{\mathrm{m}}}\nu_{ji_{\mathrm{p}}}^{\mathrm{p}}A_j^{\mathrm{m}} = M_{i_{\mathrm{p}}} \qquad K_{i_{\mathrm{p}}}^{\mathrm{p}} = \prod_{j=1}^{N_{\mathrm{m}}}\left(\gamma_j^{\mathrm{m}}c_j^{\mathrm{m}}\right)^{-\nu_{ji}^{\mathrm{p}}}$	[1.7]
	Chemical Kinetic Reactions	
General rate equation for aqueous species	$\frac{\mathrm{d}c_i}{\mathrm{d}t} = \sum_{j_{\mathrm{k}}=1}^{N_{\mathrm{k}}}\nu_{j_{\mathrm{k}},i}^{\mathrm{k}}R_{j_{\mathrm{k}}}$	[1.8]
Mineral dissolution equation (Lasaga, 1995)	$R_{j_{\mathrm{k}}} = k_0 A_{\min}\exp\left(-E_{\mathrm{a}}/RT\right)a_{\mathrm{H}^+}^{n_{\mathrm{H}^+}}g(I)\prod_i a_i^{n_i}f\left(\Delta G_r\right)$ affinity term based on transition state theory (Aagaard and Helgeson, 1982; Lasaga, 1981, 1995, 1998): $f\left(\Delta G_{\mathrm{r}}\right) = 1 - Q/K_{i_{\mathrm{p}}}^{\mathrm{p}}$	[1.9]
Monod rate equation (Schäfer et al., 1998)	$R_{j_k} = v_{\max,j_k}X_{\mathrm{mo},r}\prod_{m=1}^{N_{M,j_k}}\frac{c_{j_k,m}}{K_{j_k,m}^{M} + c_{j_k,m}}\prod_{i=1}^{N_{I,j_k}}\frac{K_{j_k,i}^{I}}{K_{j_k,i}^{I} + c_{j_k,m}}$	[1.10]

† Symbols are defined in the Appendix.

The conservation of solute mass combined with Fick's law of diffusion results in the advection–dispersion equation as given by Eq. [1.3] in Table 1. This equation is not only applicable to dissolved chemical elements, but also to colloids (e.g., van Genuchten and Šimůnek, 2004; DeNovio et al., 2004; Šimůnek et al., 2006) and microorganisms (e.g., Taylor and Jaffé, 1990; Jin et al., 2002; Rockhold et al., 2004, 2005; Gargiulo et al., 2007). Note that Eq. [1.3] in Table 1 is expressed in terms of the total concentration C [mol L^{-1}] of a given component j:

$$C_j = c_j + \sum_{i=1}^{N_{\mathrm{sa}}}\nu_{ji}c_i \qquad [1]$$

where c_j is the concentration of the jth component, c_i is the concentration of the ith secondary species, ν_{ji} is the stoichiometric coefficient of the jth component in the reaction equation for the ith species, and N_{sa} is the number of secondary species. Equation [1.3] is based on the assumption that diffusion coefficients of all species are equal (see also Lichtner, 1996; Mayer, 1999). The $R_{\mathrm{o},j}$ term in Eq. [1.3] represents sources–sinks for components in the aqueous phase, accounting for various heterogeneous equilibrium and kinetic reactions and homogeneous kinetic reactions. Depending on the type of component, different reactions and processes will be involved.

Heterogeneous reactions involve chemical elements in other than the liquid phase and include adsorption reactions described

by adsorption isotherms (linear, Freundlich, or Langmuir isotherms), cation exchange (e.g., Voegelin et al., 2001; Bruggenwert and Kamphorst, 1982), or surface complexation reactions (e.g., see Goldberg et al. [2007] for a review of soil systems), mineral dissolution–precipitation, and gas dissolution–exsolution. Except for adsorption reactions described by isotherms, the other three types of reactions, together with aqueous speciation, account for multicomponent interactions. Their equilibrium state is determined by mass-action laws such as given by Eq. [1.4–1.7] in Table 1. See Morel and Hering (1993), Langmuir (1997), and Appelo and Postma (2005) for background on activities, exchange conventions, and surface complexation models. Heterogeneous equilibrium is obtained by inserting the number of moles of the species (derived from the mass-action equations) into the mole- and charge-balance equations. Heterogeneous reactions can also be treated kinetically (e.g., Dang et al., 1994; Tebes-Stevens et al., 1998).

Kinetic homogeneous reactions are reactions that occur solely in the liquid phase and include radioactive decay, biologically mediated degradation, and solute uptake by roots (Barber, 1995; Tinker and Nye, 2000; Hopmans and Bristow, 2002; Nowack et al., 2006). Examples of complex kinetic rate equations are mineral dissolution and precipitation rates based on transition-state theory (e.g., Lasaga, 1995; Mayer et al., 2002), Monod-type rate equations (e.g., Schäfer et al., 1998; Salvage and Yeh, 1998), and biofilm models (e.g., Cunningham and Mendoza-Sanchez, 2006) for biodegradation and microbial growth such as those given by Eq. [1.8–1.10] in Table 1.

Additional heterogeneous reactions may occur for colloids and microorganisms, such as attachment–detachment processes at the solid phase, straining, filtration, partitioning of colloids to the air–water interface, and size exclusion (e.g., Wan and Tokunaga, 1997, 2002; Bradford et al., 2003, 2006; Šimůnek et al., 2006; Gargiulo et al., 2007). Biomass production and decay are other important processes that need to be taken into account when predicting the fate of microorganisms in soil systems.

Feedback

The heat transport equation (Eq. [1.2]) is coupled to the Richards equation (Eq. [1.1]) through the effects of the fluid flux on heat advection and the apparent thermal conductivity. Conversely, temperature affects surface tension, viscosity, and fluid density and, consequently, the soil hydraulic properties (e.g., Zhang et al., 2003).

Integrating the water flow and advection–dispersion equations into one numerical tool allows one to account for the effects of water flow on solute fate and transport. Solute advection and hydrodynamic dispersion are directly influenced by water fluxes, while many chemical and biological reactions depend strongly on water contents. Water contents also indirectly influence soil O_2 and CO_2 concentrations, which have a direct effect on pH and consequently on many chemical and biological reactions and processes. Although CO_2 transport and production processes are considered in HYDRUS-1D, they have not yet been incorporated into HP1. Solute concentrations affect the density of the liquid phase and can also influence root water uptake due to salinity stress (van Genuchten, 1987; Hopmans and Bristow, 2002). Soil temperatures may be affected by heat produced or consumed during various geochemical and biological reactions. The reverse feedback (i.e., the effect of temperature on solute transport and reactions) is, however, much more important. Solute transport and reactions additionally are strongly affected by the temperature dependence of the diffusion coefficient and by thermodynamic constants and reaction rates.

How and what processes are incorporated into the reaction term may have a considerable effect on the predicted mobility of various components. Many unsaturated flow and transport models coupling water flow and solute and heat transport incorporate reaction terms for single components to account for such reactions as equilibrium or nonequilibrium sorption by using linear, Freundlich, or Langmuir isotherms and first- or zero-order kinetics. In these types of models, the concentration of one element has no effect on the fate of other elements except when considering a sequential decay reaction. By including interactions between different components, one can calculate aqueous speciation, competitive adsorption described by cation exchange or surface complexation reactions, or complex kinetic reactions (see Table 1). Aqueous speciation can enhance the apparent solubility, adsorption potential, and mobility of some of the elements due to cation–ligand complexation. Examples of such complexation reactions are U complexes (Waite et al., 1994; McKinley et al., 1995; Morrison et al., 1995; Lenhart and Honeyman, 1999; Lenhart et al., 2000; Barnett et al., 2002) or the formation of soluble Al– or Fe–organic matter complexes (Jansen et al., 2002; Carrillo-González et al., 2006). As discussed above, variably saturated flow affects many geochemical variables (e.g., pH, concentrations) that consequently influence geochemical equilibrium. A linear equilibrium single-component adsorption model in which the solute distribution between the liquid and solid phases is described using the distribution coefficient, K_d, leads to completely different concentration patterns than those predicted using a competitive cation exchange model (e.g., Gonçalves et al., 2006) or a surface-complexation model (Zhu, 2003). This is due to the inability of the K_d approach to account for spatial and temporal variations in the soil water chemistry and water contents. These variations lead to changes in the ratio between exchanger and fluid content and consequently affect competition between cations for the exchange complex (Steefel et al., 2005).

An important feedback of geochemical reactions on transport processes is the effect of mineral dissolution and precipitation on not only the overall porosity of the system, but also on the pore-size distribution. This feedback affects all transport-related soil properties. These properties or parameters can be updated in various ways. For example, diffusion coefficients can be evaluated using Archie's law by introducing a cementation factor (Soler and Lasaga, 1998; van der Lee et al., 2003), while saturated hydraulic conductivities can be modified using macroscopic or grain-scale models (e.g., Le Gallo et al., 1998), and the unsaturated hydraulic properties using various physical models (Freedman et al., 2004) or pedotransfer functions (Finke, 2006).

In addition to geochemical reactions, microbial colonization and microbially produced compounds can also significantly impact the hydraulic regime. Microbial processes, for example, may lower the capillary fringe or induce locally dry zones (Yarwood et al., 2006). Microbial processes can affect not only the physical properties of a porous medium by clogging pores, producing capsules, or generating gases, but also the air–liquid interfacial tension or the solid–liquid contact angle due to the production of surface-

active compounds (Yarwood et al., 2006). Rockhold et al. (2002) modeled such changes by using pressure head scaling factors. Several of the processes and feedbacks discussed here (notably the effects of chemical precipitation–dissolution and microbial growth on porosity and pore size distribution and CO_2 transport and production) are not yet included into the current version of the HP1 simulator (Jacques and Šimůnek, 2005).

Case Study: Uranium Leaching from Soils Following Long-Term Mineral Phosphorus Fertilization

Background

Common inorganic phosphate fertilizers such as triple superphosphate, single superphosphate, monoammonium phosphate, and diammonium phosphate are produced from apatite, $Ca_5(PO_4)_3(OH,F,Cl)$. Both PO_4^{2-} and Ca during production are replaced by other elements such as radionuclides from the ^{238}U and ^{232}Th decay series (mainly ^{226}Ra and ^{210}Pb) and rare earth elements originating from the original raw material (Saueia and Mazzilli, 2006). Phosphoric acid and the byproduct phosphogypsum are produced using H_2SO_4 according to the following reaction:

$$Ca_{10}F_2(PO_4)_6 + 10\ H_2SO_4 + 10\ H_2O \rightarrow 10\ CaSO_4{\cdot}2H_2O + 6\ H_3PO_4 + 2\ HF \quad [2]$$

Phosphogypsum (a calcium sulfate dihydrate) is often enriched with ^{226}Ra because of its chemical similarity to Ca (Papastefanou et al., 2006, Santos et al., 2006). Phosphoric acid produced during the phosphate production process reacts with phosphate rocks to yield monocalcium phosphate or triple superphosphate, with overall reactions as follows (Saueia and Mazzilli, 2006):

$$Ca_{10}F_2(PO_4)_6 + 7\ H_2SO_4 + 6.5\ H_2O \rightarrow 3\ Ca(H_2PO_4)_2{\cdot}H_2O + 7\ CaSO_4.0.5H_2O + 2\ HF \quad [3]$$

$$Ca_{10}F_2(PO_4)_6 + 10\ H_3PO_4 + 10\ H_2O \rightarrow 10\ Ca(H_2PO_4)_2{\cdot}H_2O + 2\ HF \quad [4]$$

Compared with phosphate rock, the mineral P fertilizers are enriched in U since U remains in the liquid phase together with H_3PO_4 during the acidification of the phosphate rock. The U concentration of the P fertilizer is related to the amount of the phosphate in the fertilizer (Barišić et al., 1992). Uranium concentrations in P-bearing fertilizers have been reported to be in the range of 300 to 3000 Bq kg^{-1} of fertilizer (European Commission, 1999), or 1700 to 9200 Bq kg^{-1} of fertilizer for both ^{238}U and ^{234}U (Cogné, 1993).

The environmental and radiological impacts of the application of inorganic P fertilizers are, in general, relatively modest. Spalding and Sackett (1972) attributed the increase of U in North American rivers to applications of large amounts of P fertilizers to agricultural lands. Rothbaum et al. (1979) found that most U originating from applied superphosphate was retained within the plow layer of arable soils or in the organic surface layers under grassland. Barišić et al. (1992) concluded that >20% of the annually deposited U by fertilizers is transported to drainage channels in the Kanovci area of the Republic of Croatia. Their data indicated that high U concentrations in surface waters and shallow groundwater were caused by phosphate fertilizer applications. On the other hand, Zielinski et al. (1997) found that leaching of U from inorganic P fertilizers contributed much less to high U concentrations in drainage water than natural or irrigation-enhanced leaching from soils. The radiological impact expressed as dose is also quite limited (Saueia and Mazzilli, 2006).

Zielinski et al. (1997) pointed out that the mobility and the nature of P and U fixation and precipitation depend on soil conditions, such as pH, moisture, mineralogy, and texture. Guzman et al. (2002) provided a number of processes controlling U mobility. The list included sorption on solid surfaces, formation of complexes with Ca, PO_4^{2-}, and CO_3^{2-}, and (co-)precipitation of U–P, Ca–U, Al–P, or Fe–P (acid soils) or Ca–P (alkaline soils) minerals (see also Zielinski et al., 1997; Brady, 1990).

To model the subsurface transport of U, either naturally occurring in soils or applied with mineral fertilizers, the interaction of U with other elements and the solid phase needs to be considered. The amount of U adsorption to the solid phase depends on the specific composition of both the solid phase (e.g., clay minerals, Fe and Al oxides, and organic matter) and the aqueous phase (e.g., pH, complexing agents such as Cl^-, SO_4^{2-}, PO_4^{2-}, or the presence of competing cations for cation exchange or surface complexation). The amount of Fe oxides in the soil strongly affects the pH dependence of U sorption (Barnett et al., 2000). Changing chemical conditions significantly influences the mobility of U in soils and sediments (Kohler et al., 1996). Here we use HP1 to obtain insight into the complex system of interacting geochemical processes that govern Ca, P, and U mobility in the soil when an inorganic P fertilizer is applied annually. Our study is an update of preliminary calculations by Jacques et al. (2006a). We focus especially on the effects of the imposed upper boundary condition (constant vs. transient atmospheric boundary conditions) on the migration of U in an undisturbed acid soil profile. The analysis of migration of Ca, P, and U is performed in terms of temporal variations in the distribution coefficient K_d to illustrate the limitation of such an empirical approach, which was illustrated in previous studies by Bethke and Brady (2000), among others.

Problem Definition

Phosphorus fertilizers are often applied annually to agricultural fields, partly in inorganic form. In Flanders (northern Belgium), the amount of applied P that originates from mineral fertilizers decreased from 13.9×10^6 kg P in 1990 to 2.38×10^6 kg P in 2003 (MIRA Team, 2004). To simulate the long-term migration of P and U through the soil, the following assumptions were made: (i) an average P fertilization of 1 g P m^{-2} (or 6.35×10^6 kg P for all of Flanders) is applied each year on 1 May in the form of $Ca(H_2PO_4)_2$; and (ii) 1 kg of $Ca(H_2PO_4)_2$ contains 10^{-3} mol of U. Based on a specific activity 2.96×10^6 Bq mol^{-1} U, 2960 Bq of alpha activity exclusively due to ^{238}U is present in 1 kg of $Ca(H_2PO_4)_2$. Thus, a fertilization of 1 g P m^{-2} corresponds to 1.61×10^{-2} mol of $Ca(H_2PO_4)_2$ containing 3.77×10^{-6} mol of U.

The soil profile studied here is a dry Spodosol located at the "Kattenbos" site (Lommel, Belgium) consisting of seven soil

horizons in the top 1 m. The soil has a typical leached E horizon between 7 and 19 cm below the surface and enriched (in organic matter and Fe oxides) Bh horizons between 19 and 28 cm. We note that the top horizons are not typical for an agricultural soil, but rather reflect an undisturbed profile covered by natural vegetation (i.e., heather). The profile was selected for our modeling purposes because it was well characterized in terms of physical and geochemical properties. Table 2 gives the locations of the different soil horizons and their soil hydraulic parameters as determined on undisturbed soil samples of 100 cm^3 (Seuntjens, 2000; Seuntjens et al., 2001a).

TABLE 2. Soil hydraulic parameters† (van Genuchten, 1980) of the dry Spodosol (data from Seuntjens [2000] and Seuntjens et al. [2001a]).

Horizon‡		Depth	θ_r	θ_s	α	n	K_s
		cm			m^{-1}		$m\ s^{-1}$
Top mineral layer, A		0–7	0.065	0.48	1.6	1.94	1.1×10^{-5}
Elluviated layer, E		7–19	0.035	0.42	1.5	3.21	3.6×10^{-5}
Illuviated layer with organic matter	Bh1	19–24	0.042	0.47	1.6	1.52	4.5×10^{-6}
	Bh2	24–28	0.044	0.46	2.8	2.01	1.0×10^{-4}
Transition layer, BC		28–50	0.039	0.46	2.3	2.99	1.4×10^{-4}
Unconsolidated material	C1	50–75	0.030	0.42	2.1	3.72	1.4×10^{-4}
	C2	75–100	0.021	0.39	2.1	4.33	1.4×10^{-4}

† θ_r and θ_s are the residual and saturated water contents, respectively; α and n are shape parameters; and K_s is saturated hydraulic conductivity.
‡ Description from Brady (1990).

Our conceptual chemical model considers the transport of the following 14 components: the elements C, Ca, Cl, F, Mg, N(V), Na, P, S(VI), and U(VI), H_2O, O (not included in water), H (not included in water), and the charge of the soil solution. Normally a solution is always charge balanced; however, in a model that includes surface reactions without compensating the surface charge in the diffuse double layer, both the aqueous phase and the solid surface will have a charge of opposite sign. The total system must still be charge balanced.

Three types of geochemical equilibrium reactions were taken into account: (i) aqueous speciation reactions; (ii) cation exchange reactions on organic matter; and (iii) surface complexation reactions on Fe oxides. The thermodynamic data for the aqueous species were taken from the WATEQ4F database (Ball and Nordstrom, 1991), complemented with data for U from Langmuir (1997).

The cation exchange complex was assumed to be associated solely with organic matter. Organic matter typically consists of an assemblage of different functional groups and types of adsorption sites. A multisite cation exchange complex allows simulations of the acid–base properties of the organic matter and the corresponding increase in the cation exchange capacity with increasing pH (e.g., Appelo et al., 1998). Appelo et al. (1998) included proton exchange on a multisite cation exchange complex to mimic the presence of different functional groups. Six cation exchangers were assumed to be present, each with a different K^c value for the half reaction for H^+:

$$Y_i + H^+ = HY_i \qquad [5]$$

where Y_i is a cation exchange site (i = a, b, c, d, e, f). Table 3 gives the K^c values for the multisite exchange complex. Depending on the pH, some sites are deprotonated such that cations can adsorb. Other sites, however, will remain protonated and are thus not available for cation exchange. Besides H^+, five cation species (Na^+, K^+, Mg^{2+}, Ca^{2+}, and UO_2^+) participated in the exchange reactions. The exchange coefficients for the cations were assumed to be the same on all six sites. The size of the total cation exchange complex was estimated from the organic matter content and the amount of exchangeable protons on the organic matter. The proton dissociating groups on fulvic and humic acids are between 6 and 10 $mol_c\ kg^{-1}$ and between 4 and 6 $mol_c\ kg^{-1}$ organic matter, respectively (Tipping, 2002). We used an average value of 6 $mol_c\ kg^{-1}$ organic matter.

Both cations and anions adsorb on Fe oxides. Adsorption was described by specific binding using a nonelectrostatic surface complexation model. Surface complexation reactions included surface hydrolysis reactions (protonation and deprotonation) and reactions involving the cations Ca^{2+}, Mg^{2+}, and UO_2^+ and the anions PO_4^{2-}, SO_4^{2-}, and Fe^- (denoting ≡FeOH as a neutral Fe oxide surface) as follows: $\equiv FeOH_2^+$, $\equiv FeO^-$, $\equiv FeH_2PO_4$, $\equiv FeHPO_4^-$, $\equiv FePO_4^{2-}$, $\equiv FeSO_4^-$, $\equiv FeOHSO_4^{2-}$, ≡FeF, $\equiv FeHF^-$, $\equiv FeOMg^+$, $\equiv FeOCa^+$, and $\equiv FeOUO_2^+$. Equilibrium constants for weak sites were taken from Dzombak and Morel (1990) (see also Parkhurst and Appelo, 1999). The capacity of the surface was derived from the amount of Fe_2O_3 as measured in the soil profile assuming 0.875 reactive sites per mole of Fe (Waite et al., 1994). The cation exchange capacity and the reactive sites of each horizon are given in Table 4.

Although CO_2 in general is important for U speciation, this type of complexation reaction is not important in our simulations since the pH varied only between 3.5 and 4.5. The partial pressures of O_2 and CO_2 in the soil air phase were assumed to be constant and equal to 20 and 0.32 kPa, respectively. These values are smaller and larger, respectively, than the partial pressures in the atmosphere. The assumption of having a constant CO_2 partial pressure represents a significant simplification since soil CO_2 concentrations in general display strong seasonal variations related to the microbiological activity in the soil (e.g., Šimůnek and Suarez, 1993; Suarez and Šimůnek, 1993).

Meteorological data from two weather stations (from Brogel for years 1969–1985 and from Mol/Geel for 1986–1998) were used to define precipitation, P [$L\ T^{-1}$], and potential evaporation, E_p [$L\ T^{-1}$], rates, the latter based on the Penmann equation

TABLE 3. Logarithmic equilibrium constants (K^c) parameters for the multisite exchange complex.

Y-	NaY	KY	MgY_2	CaY_2	UO_2Y_2	
Exchanger†	−1.0	−0.3	−0.4	−0.2	−0.2	
HY‡	HYa	HYb	HYc	HYd	HYe	HYf
	1.65	3.3	4.95	6.85	9.6	12.35

† The value for NaY was taken from Appelo et al. (1998). Values for the other complexes were taken from the phreeqc.dat database (Parkhurst and Appelo, 1999) and adapted relative to the K for NaY.
‡ Values taken from Appelo et al. (1998).

TABLE 4. Bulk densities, weight contents of organic matter and Fe_2O_3 of the dry Spodosol (Seuntjens et al., 2001a; Seuntjens, 2000), and calculated sizes of the multisite cation exchange complex (CEC) and the Fe-oxide surfaces.

Horizon	Bulk density	Organic matter	Fe_2O_3	CEC	Sites on surface
	g cm^{-3}	%		mol$_c$ m^{-3} soil	
A	1.31	3.65	0.20	287	28.7
E	1.59	0.78	0.09	74	15.7
Bh1	1.30	3.03	1.19	236	169.5
Bh2	1.38	1.23	1.19	102	180.0
BC	1.41	0.55	0.68	46	105.1
C1	1.52	0.30	0.57	27	94.9
C2	1.56	0.13	0.57	12	97.4

(Penmann, 1948). Statistical information about the imposed climatological time series is given in Jacques et al. (2008). To obtain a 200-yr time series for modeling purposes, the 30-yr period was simply repeated several times. A free-drainage boundary condition was assumed at the bottom of the soil profile.

Element concentrations in the rainwater were obtained from Stolk (2001) for Station 231 located in Gilze-Rijen (the Netherlands), which is sufficiently close to the investigated site. The solution composition was based on the average of 13 measurements during 1999 (Table 5). The U concentration of the rainwater was set equal to an arbitrary low value of 10^{-24} mol L^{-1} to have the required non-zero initial concentration for PHREEQC simulations. The P fertilizer was assumed to be applied every year on 1 May in the form of $Ca(H_2PO_4)_2$ in 1 cm of irrigation water with the same composition as rainwater. The fertilizer was assumed to be completely dissolved in the irrigation water, thus neglecting any possible kinetics in the dissolution process of the fertilizer grains. Before the 200-yr simulation, a 5-yr steady-state flow simulation was performed without fertilizer applications to establish chemical initial conditions in topsoil horizons in equilibrium with the chemistry of the inflowing rainwater.

Simulation Results

Speciation of Phosphate, Uranium, and the Solid-Phase Surfaces

Aqueous speciation of U and P in the soil solution was calculated with PHREEQC between pH 2 and 6 for the rainwater composition, the selected soil air partial pressures of O_2 and CO_2, and an assumed aqueous U concentration of 8.0×10^{-9} mol L^{-1}. This value corresponds with the average U concentration at 5-cm depth obtained after 50 yr in the steady-state flow simulations. When the background P concentration in rainwater is the only P source, UO_2^{2+} is the dominant U species in the soil solution, followed by UO_2F^+, UO_2SO_4, UO_2OH^+, and UO_2HPO_4. When the P concentration is much higher due to the addition of the P fertilizer, UO_2^{2+} is still the dominant U species, followed by $UO_2HPO_4^-$ (dominant at pH values >4), UO_2F^+, and UO_2OH^+. For both cases, $H_2PO_4^-$ was the most abundant aqueous P species, followed by H_3PO_4.

Surface speciation was also calculated for the same pH range, the rainwater composition, the soil air partial pressures of O_2 and CO_2, and the total aqueous U concentration of 10^{-9} mol L^{-1}. The Na concentration was adapted to obtain the required pH and charge balance. Figure 1a shows the most abundant surface species on the Fe oxides. The surface of the Fe oxides was mostly protonated. Below pH 5.5, FeH_2PO_4 was the second most abundant surface species. The amounts of FeOH, $FeHPO_4^-$, and $FeOUO_2^+$ increased substantially across the considered pH range. For example, $FeOUO_2^+$ increased up to seven orders of magnitude. The amount of adsorbed U consequently also increased

TABLE 5. Composition of the rainwater (Stolk, 2001) and rainwater with P fertilizer.

Element	Rainwater	Rainwater + P fertilizer
	mol L^{-1}	
C(4)	1.45×10^{-5}	1.45×10^{-5}
Ca	6.00×10^{-6}	1.62×10^{-3}
Cl	6.95×10^{-5}	6.95×10^{-5}
F	1.00×10^{-6}	1.00×10^{-6}
K	4.00×10^{-6}	4.00×10^{-6}
Mg	8.00×10^{-6}	8.00×10^{-6}
N(V)	3.70×10^{-5}	3.70×10^{-5}
Na	6.40×10^{-5}	6.40×10^{-5}
P	7.00×10^{-7}	3.22×10^{-3}
S(VI)	3.10×10^{-5}	3.10×10^{-5}
U(VI)	1.00×10^{-24}	3.77×10^{-7}
pO_2(g), Pa	2.07×10^{4}	2.07×10^{4}
pCO_2(g), Pa	3.20×10^{1}	3.20×10^{1}
pH	4.1	4.2

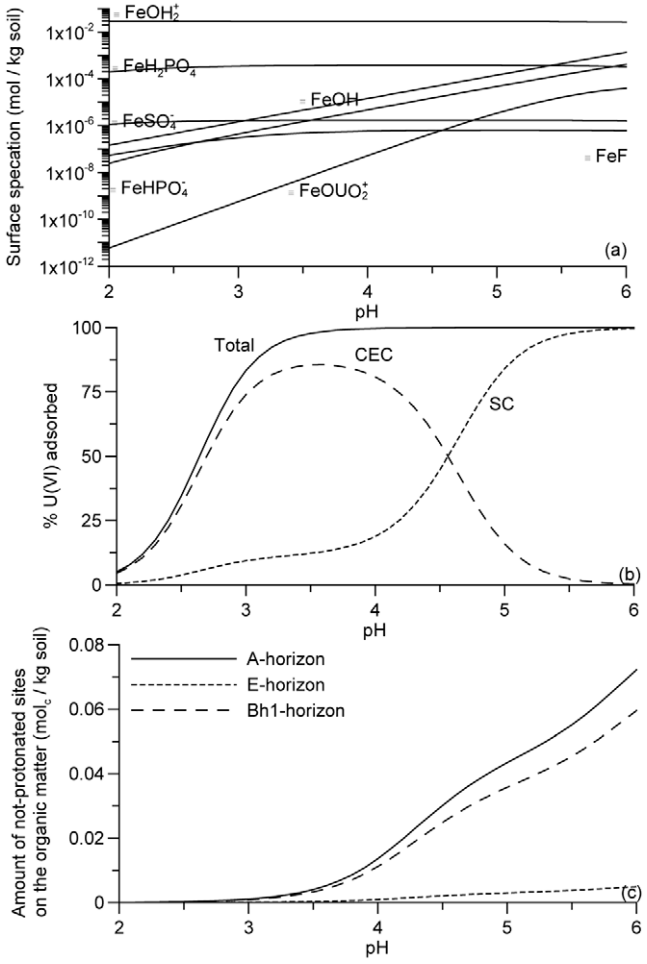

FIG. 1. (a) Surface speciation (Fe oxides) as a function of pH, (b) pH dependency of the adsorption of U(VI) in the A horizon on both the cation exchange complex (CEC) and the surface complex (SC), and (c) pH dependency of the size of the cation exchange complex on organic matter for the A, E, and Bh1 horizons of the dry Spodosol.

drastically. Figure 1b shows the ratio of total adsorbed U to total U in the system together with the distribution of U between the two sorption processes involved (i.e., cation exchange on organic matter and surface complexation on Fe oxides). Almost all U was in solution at low pH since both the cation exchange complex and the surface sites were mostly protonated. While about 50% of the total U was adsorbed around pH 3, almost all U was adsorbed at pH 4. The relative contribution of U adsorbed by cation exchange compared with surface complexation decreased with increasing pH. This is consistent with the experimental findings of McKinley et al. (1995). We found that U adsorption on the cation exchange complex increased up to pH 4.7 (results not further shown). Since the Na concentration in solution increases with increasing pH owing to the Na addition for the purpose of obtaining charge balance, Na will increasingly replace the other cations on the exchange complex at higher pH. Note that above pH 6, U adsorption will decrease again when dissolved CO_2 is present due to the formation of U(VI)–CO_3 complexes (Davis et al., 2004a; Waite et al., 1994). Almost all P was adsorbed in the studied pH range, with 99.3 and 99.8% P being adsorbed at pH 2 and 6, respectively (results not shown).

The soil horizons differed in their adsorption capacity, as illustrated in Fig. 1c and Fig. 2. Figure 1c shows the increasing capacity of the exchange complex to retain cations other than protons with increasing pH. This capacity was lowest for the E horizon due to the low organic matter content. Figure 2 shows K_d values defined as the total adsorbed Ca, P, and U concentrations (mol kg^{-1}) across the aqueous Ca, P, and U concentrations (mol L^{-1}), respectively, for the A, E, and Bh2 horizons. The horizons had different sorption types and capacities: the A horizon had a high capacity of the exchange complex and a low capacity of the surface complex, the E horizon had low capacities of both the exchange and surface complexes, while the Bh2 horizon had the highest capacity of the surface complex. The K_d values are shown for two aqueous-phase compositions: rainwater without the P fertilizer (having an aqueous U concentration of 8×10^{-9} mol L^{-1} for the A and E horizons and 4 x10^{-9} mol L^{-1} for the Bh2 horizon representative of the long-term averaged U concentrations during the steady-state flow simulation) and rainwater with the P fertilizer (Table 5). The pH was controlled by changing the Na and Cl concentrations. The K_d values of Ca and U were both strongly pH dependent, whereas the K_d of P was relatively independent of pH.

The composition of soil water had a significant effect on the K_d value. Since the concentrations of Ca, P, and U were much larger when rainwater infiltrated following P-fertilizer application, competition for the same number of sites on the cation exchange and surface complexes increased and more elements remained in the aqueous phase. At pH 4, this resulted in a decrease in K_d of almost two orders of magnitude for Ca and P, and a decrease of about three orders of magnitude for U. Accordingly, the percentages of U and P adsorbed in the A horizon ranged from 1.5 to 41% for U and from 89.6 to 89.8% for P (results not shown). Note that almost 100% of U was adsorbed when rainwater in the absence of P fertilizer infiltrated into the soil (Fig. 1b). A slight decrease in K_d for U occurred between pH 3.5 and 4.5, especially in the A and E horizons for rainwater with the P fertilizer. For the A horizon, the first maximum in the percentage of adsorbed U was around pH 3.4 (33%), with mainly sorption on the cation exchange complex (results not shown). This is different from the case for rainwater without P fertilizer when already >10% of the total amount of U was sorbed onto the surface complex (Fig. 1b). The K_d reached a minimum at pH 4.7 in the A horizon (Fig. 2a), with only 13% of the total U amount adsorbed on the exchange and surface complexes (6.5% on both the cation and surface complexes). From pH 4.7 to 6, the percentage of U adsorbed on the surface complex increased to 42%. The small capacity of the surface complex and the high concentration of competing species (especially P) resulted in a shift in U adsorption on the surface complex toward higher pH values. This effect was less pronounced in the Bh horizon because of its higher capacity of the surface complex.

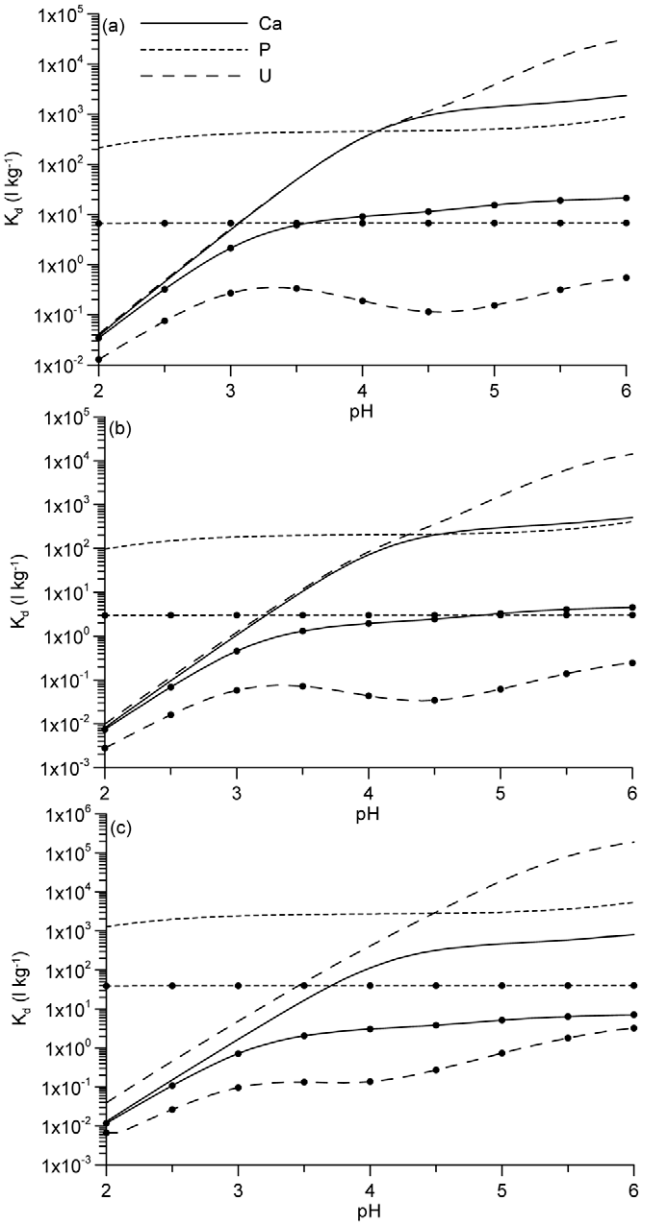

FIG. 2. The linear distribution coefficient, K_d, of Ca, P, and U as a function of pH for rainwater with a U concentration of 8.0×10^{-9} mol L^{-1} for the A and E horizons and 4.0×10^{-9} mol L^{-1} for the Bh2 horizons (lines without dots) and for rainwater with the P fertilizer (lines with dots) for the (a) A, (b) E, and (c) Bh2 horizons.

Different solution compositions affect the relative mobility between Ca, P, and U. For rainwater without P fertilizer, U was less mobile than P at pH values above 4.3 to 4.5, depending on the soil horizon; however, U was always more mobile when the rainwater contained P fertilizer. The relative mobility of P and Ca did not depend only on the water composition, but also on the soil horizon. In the A horizon with a high exchange capacity and low surface complex capacity, Ca was less mobile than P at pH values >4.3 for rainwater without P fertilizer and 3.5 for rainwater with P fertilizer. In the Bh2 horizon with a relatively high surface complex capacity, the K_d of P was always larger that the K_d of Ca.

Calcium, Phosphorus, and Uranium Depth Profiles

Figure 3 shows distributions vs. depth of total Ca, P, and U per cubic meter of soil at selected times for both the steady-state and transient water flow simulations. Total concentrations were obtained by summing the amounts in the aqueous phase, on the cation exchange complex (for Ca and U), and on the surface complex (for Ca, U, and P). Note the different concentration scales for P in plots for the first 50 and the last 150 yr. Calcium accumulated mainly in the upper horizon during the first 50 yr, although more accumulated in the Bh1 horizon under transient-flow conditions. During the next 100 yr, the amount of Ca in the two Bh horizons gradually increased. This occurred somewhat faster for the transient than the steady-state simulation. After 200 yr, however, the amount of Ca in the top 50 cm was quite similar for the two cases.

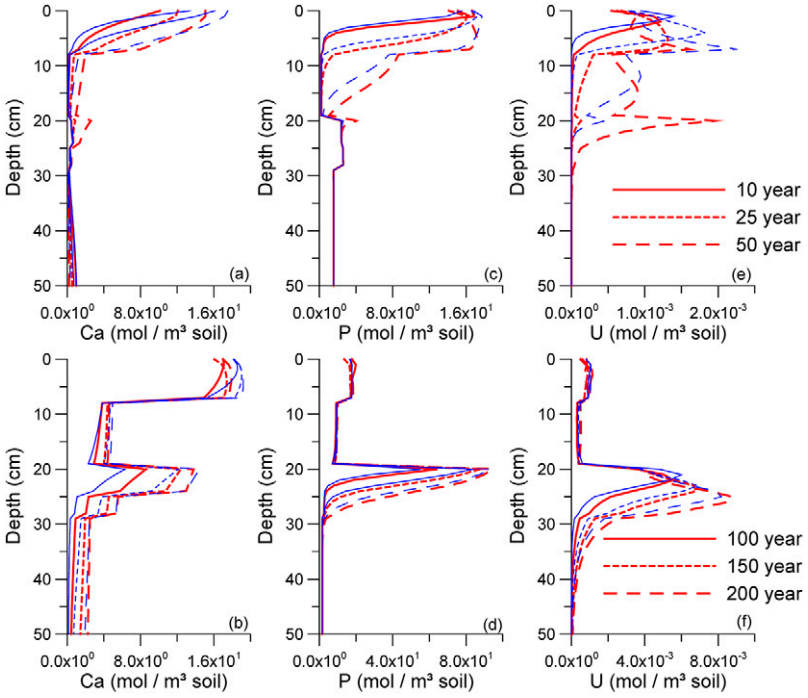

FIG. 3. Concentration profiles vs. depth of total (a and b) Ca, (c and d) P, and (e and f) U at (a, c, and e) 10, 25, and 50 yr and (b, d, and f) 100, 150, and 200 yr for steady-state (thin blue lines) and transient (red thick lines) flow simulations. Notice the different concentration scales for P in the top and bottom plots.

Phosphorus migrated faster through the A and E horizons than did Ca (Fig. 3a vs. 3c) and was more mobile in these two horizons since the amount of Fe_2O_3 was very small. On the other hand, Ca transport was retarded by cation exchange reactions in the organic-matter-rich A horizon. The migration of P through the Bh horizons was slower than that of Ca due to strong sorption of P on the Fe oxide surface. Phosphorus had not yet reached the BC horizon after 200 yr. Note that the concentration front for the transient simulation moved slightly faster than for the steady-state flow simulation.

Uranium showed the largest differences between the two simulations, especially during the first 50 yr. Uranium migrated relatively fast, similar to P, through the A and E horizons. As discussed with Fig. 2, U was more mobile than P when the pH was <4.3, especially at relatively high Ca and P concentrations. Much U accumulated in the Bh horizon during the last 150 yr. Uranium transport was again slightly faster for the transient simulation than during steady-state flow.

Temporal Variations in the Linear Distribution Coefficient

Figures 4 and 5 show time series of pH and the K_d values for Ca, P, and U at depths of 5 (A horizon) and 25 (Bh2 horizon) cm, respectively. A long-time trend in K_d was observed for both steady-state and transient flow simulations. This trend is related to long-time changes in the amount of Ca, P, and U in the soil solution due to application of the P fertilizer. Steady-state solute transport conditions are reached when K_d becomes constant for the steady-state flow simulation. This condition was reached faster for P and U (at about 40–50 yr) than for Ca (at about 100 yr) at 5-cm depth. This is similar to the conclusion drawn from Fig. 3. Since the total concentrations increased from the initial condition, the K_d at 5-cm depth decreased by almost one order of magnitude

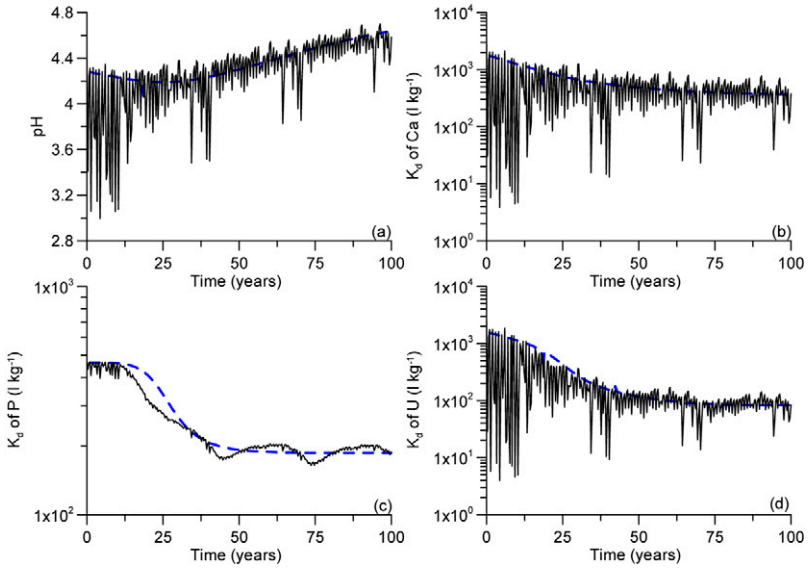

FIG. 4. Time series of (a) pH and of the linear distribution coefficient, K_d, for (b) Ca, (c) P, and (d) U at a depth of 5 cm for the steady-state (dashed blue line) and transient (solid black line) flow simulations during the first 100 yr.

for Ca, by one-third for P, and slightly more than one order of magnitude for U. The increase in competition between elements for the surface sites had a larger effect on the long-time sorption potential than the long-time pH increase on the K_d values. A different picture emerged for the Bh2 horizon at a depth of 25 cm (Fig. 5). The increase in pH during the 200-yr simulation caused here an increase in adsorption potential for U (increasing K_d). The competition with P for the surface complex was limited since P migrated more slowly through the Bh horizons than U (see Fig. 3). After 200 yr, the peak in U occurred at a depth of about 25 cm, whereas the peak in P was at 20 cm. The K_d of P at the 25-cm depth did not show a pronounced long-time trend until 175 yr, which further reflects the limited transport of P to this depth.

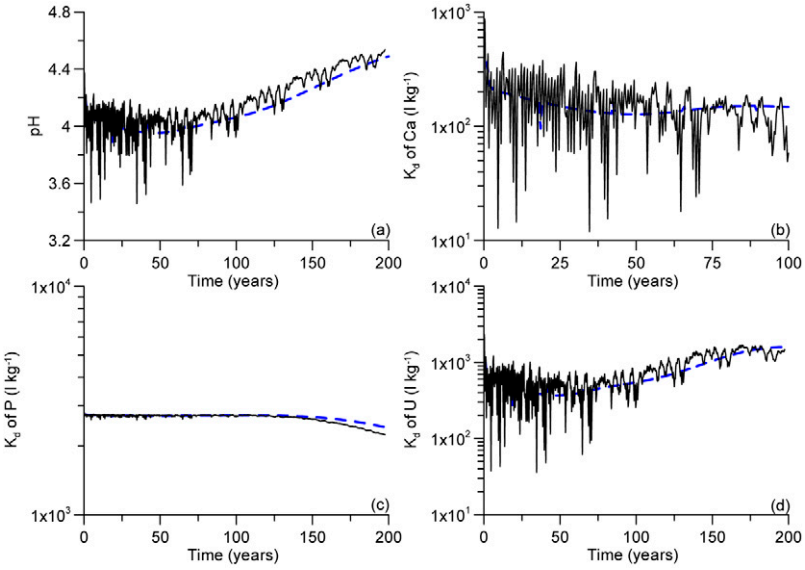

FIG. 5. Time series of (a) pH and of the linear distribution coefficient, K_d, for (b) Ca, (c) P, and (d) U at a depth of 25 cm for the steady-state (dashed blue line) and transient (solid black line) flow simulations during the first 200 yr.

The transient flow simulation showed significant short-time variations in pH and K_d for all three elements. As was discussed in Jacques et al. (2008), transient weather conditions in precipitation and evaporation resulted in variable water contents and water fluxes. These variations subsequently induced variations in geochemical conditions. Decreasing water contents due to evaporation coincided with decreasing pH because of an increase in ionic strength (Jacques et al., 2008). In this study, the decrease in pH caused, in general, the adsorption potential for Ca and U to decrease. Short-time variations in P concentrations were limited due to the pH independence of its K_d, as discussed above. Note that the repetition of a 30-yr time series of meteorological data (up to 200 yr) may result in some repetitive pattern in the K_d time series, e.g., for P at a depth of 5 cm (Fig. 4c).

The seasonal variations in pH and K_d are pronounced close to the soil surface and for early simulation times when P and U are not yet at their long-time steady state (at 5-cm depth and for the first 40 yr). The K_d values of Ca and U changed up to two orders of magnitude during the first 20 yr. Although the difference in total amounts of the three elements between the steady-state and transient flow simulations was relatively small (see Fig. 3), the aqueous concentrations differed dramatically. This may have a profound effect on processes that are dependent on aqueous concentrations, such as nutrient uptake by roots.

Fluxes in the Soil and at the Bottom of the Soil Profile

The solute mass flux density, J_s [M L^{-2} T^{-1}], is the sum of the mass flux due to advection of the dissolved solute and the mass flux due to hydrodynamic dispersion and molecular diffusion. In terms of the resident fluid concentration, C_l^r [M L^{-3}], J_s may be written as (Jury and Roth, 1990)

$$J_s = -\theta D \frac{\partial C_l^r}{\partial z} + J_w C_l^r \qquad [6]$$

where J_w is the water flux density [L T^{-1}]. Figure 6 compares downward fluxes of Ca, P, and U for the steady-state and transient flow simulations. Fluxes are shown for the bottom of the A, Bh2, and C2 horizons at depths of 7, 28, and 100 cm, respectively. Although some upward fluxes were calculated at the bottom of the A horizon during periods of low precipitation or high potential evaporation, these were not included in Fig. 6. As indicated by the K_d time series, steady-state solute transport was obtained after 40 yr for U and P and after about 100 yr for Ca at the bottom of the A horizon. For the transient flow simulation, solute fluxes continued to vary by almost three orders of magnitude after steady-state solute transport conditions were reached for the steady-state flow simulation. Downward U fluxes for the transient flow simulation were always larger than those for the steady-state flow simulation during the first 20 yr.

At the bottom of the Bh2 horizon, solute fluxes for the steady-state flow simulation started to increase after 30, 80, and 150 yr for U, Ca, and P, respectively. Uranium fluxes reached a steady-state value after approximately 100 yr. Phosphorus never reached the bottom of the soil profile, even after 200 yr. For the steady-state flow conditions, U started to leach after 120 yr, whereas Ca fluxes increased 140 yr after an initial decrease. Uranium and Ca solute fluxes for the transient flow simulation were much higher than for the steady-state simulation. Uranium reached the bottom of the soil profile after 80 yr, while Ca fluxes started to increase after about 100 yr. Similarly as for the simulated concentration profiles (Fig. 3), the U (and also Ca) fluxes increased earlier for the transient flow simulation than for the steady-state simulation. This was most obvious at the 100-cm depth. Faster leaching of all three elements was due to interactions caused by short-time variations in water contents, water fluxes, and geochemical conditions.

Conclusions

Accurate investigation of the mobility of contaminants in the vadose zone requires consideration of all pertinent physical and biogeochemical processes. Coupling of fluid flow, advective–dispersive transport, and multicomponent geochemistry into one integrated simulator provides a much-needed tool for studying the interplay between different processes, including the various nonlinear feedbacks that occur between the different processes. Variable water contents and fluid fluxes during transient flow in the vadose zone significantly affect prevailing geochemical conditions such as soil pH. Consequently, the adsorption potential

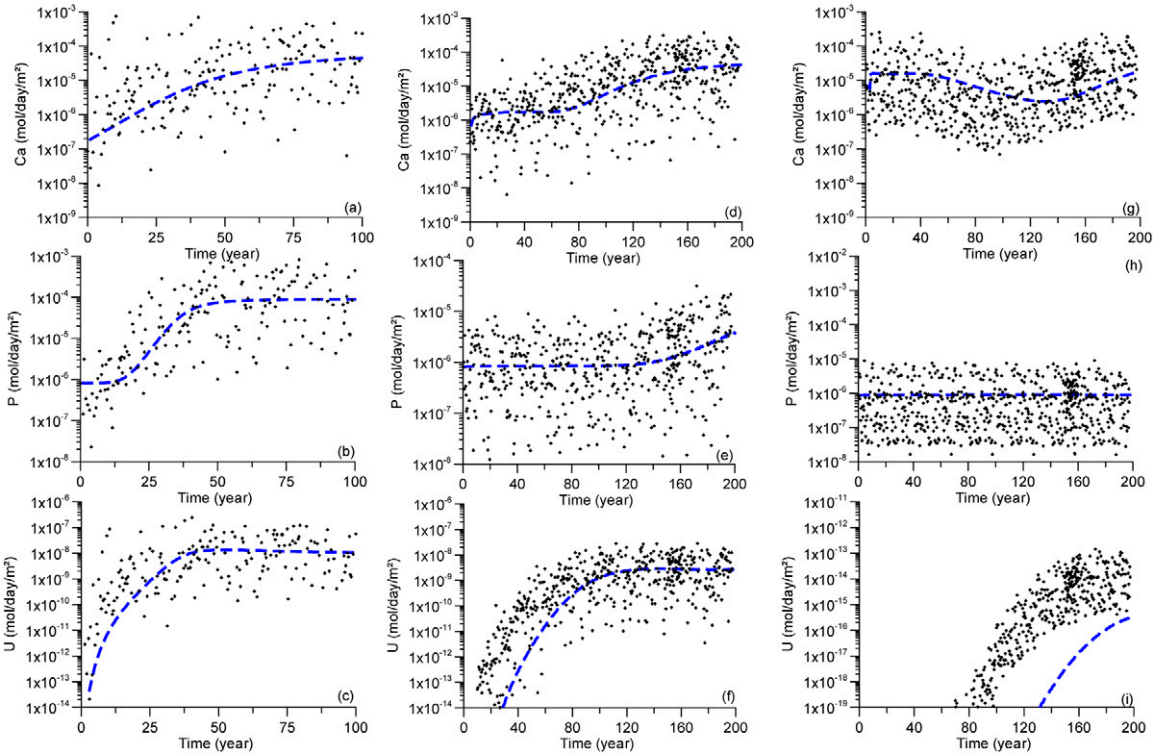

FIG. 6. Downward solute fluxes of (a, d, and g) Ca, (b, e, and f) P, and (c, f, and i) U (mol d^{-1} m^{-2}) at the bottom of the (a–c) A horizon, the (d–f) Bh2 horizon, and (g–i) the soil profile for the steady-state (dashed blue line) and transient (dots) flow simulations. Note that the time scale for the A horizon (a–c) is limited to 100 yr.

and thus the element mobility may change with time. It is similarly important for reactive transport simulators to account for interactions between different species resulting from chemical reactions such as aqueous speciation and competitive sorption on the cation exchange or surface complex. The long-time surface application of some elements (e.g., by fertilization) leads to temporal variations in the distribution coefficient K_d and a nonunique relation between K_d and pH.

We illustrated the feedbacks between the different processes, as well as the multiple interactions that may occur between the chemical species present, by using the HP1 reactive transport simulator to predict the migration of Ca, P, and U following inorganic P fertilization through a layered soil. The numerical simulations showed that the distribution coefficients for Ca, P, and U depend strongly on pH, the composition of the aqueous phase, the mineralogical properties of the soil horizons, and the amount and type of competing elements. Simulations also showed that P is a stronger competitive element for U than Ca. In horizons with large amounts of P (e.g., the A horizon), the sorption potential and K_d of U did not follow the long-term increase in pH due to the stronger counter effect of P sorption on the surface complex. On the other hand, when U and Ca reached a certain horizon (e.g., the Bh2 horizon in our example), while P did not, the K_d for U closely followed the increase in pH. Furthermore, yearly additions of Ca, P, and U in the form of P fertilizer resulted in a long-term decrease in K_d of the upper horizons. Short-term temporal variations in the water contents and fluxes, when transient flow was considered, caused significant pH variations, which produced very significant variations in the K_d values for Ca and U by up to two orders of magnitude. Leaching of Ca and U from the soil profile occurred faster in the transient flow simulation than in the steady-state simulation as a result of the interplay between changing hydrologic and geochemical soil conditions.

Appendix

a_i	activity of secondary species i (dimensionless)
A_j^{m}	chemical formula of aqueous master species j (dimensionless)
A_i	chemical formula of aqueous secondary species i (dimensionless)
A_{min}	reactive surface area [L^2]
c_i	concentration of ith aqueous species (mol kg^{-1} H_2O)
C_j	total concentration of jth component (mol kg^{-1} H_2O)
C_{p}	volumetric heat capacity of porous medium [M L^{-1} T^{-2} K^{-1}]
$C_{\mathrm{r},j}$	total concentration in the sink term (mol kg^{-1} H_2O)
C_{w}	volumetric heat capacity of the liquid phase [M L^{-1} T^{-2} K^{-1}]
D^{w}	dispersion coefficient in the liquid phase [L^2 T^{-1}]
E_{a}	apparent activation energy (kJ mol^{-1})
F	Faraday constant, 96,485 C mol^{-1}
G	Gibbs free energy (kJ mol^{-1})
h	water pressure head [L]
I	ionic strength (mol kg^{-1} H_2O)
k_0	intrinsic rate constant [mol L^{-2} T^{-1}]
K	unsaturated hydraulic conductivity [L T^{-1}]
K_y^x	equilibrium constant: superscripts x = l, e, s, or p are for aqueous, exchange, surface species, and minerals, respectively; subscript $y = i_x$ is an index for specific species (dimensionless)
$K_{j_{\mathrm{k}},i}^x$	Monod (x = M) or inhibition (x = I) constant in the ith term of degradation reaction j_{k} (mol kg^{-1} H_2O)
$M_{i_{\mathrm{p}}}$	chemical formula of mineral i_{p}
n_i	order of the reaction of secondary species i
N_{k}	number of kinetic reactions
N_{m}	number of aqueous components or master species

N_{I,j_k}	number of inhibition terms in degradation reaction j_k
N_{M,j_k}	number of Monod terms in degradation reaction j_k
q	volumetric fluid flux density [L T^{-1}]
Q	ion activity product (dimensionless)
R	universal gas constant (kJ mol^{-1} K^{-1})
R_{j_k}	rate of degradation reaction j_k [mol kg^{-1} H_2O T^{-1}]
$R_{o,j}$	source–sink term [L^3 kg^{-1} H_2O T^{-1}]
S	sink term for root water uptake [mol T^{-1}]
$S^m_{j_s}$	chemical formula of surface master species j_s
S_{i_s}	chemical formula of secondary surface species i_s
t	time [T]
T	temperature (K)
v_{max,j_k}	maximum specific rate of substrate utilization in degradation reaction j_k [mol kg^{-1} H_2O T^{-1} (mol L^{-1})$^{-1}$]
x	spatial coordinate (positive upward) [L]
$X^m_{j_e}$	chemical formula of exchange master species j_e
X_{i_e}	chemical formula of secondary exchange species i_e
$X_{mo,r}$	concentration of the microbial population r [M kg^{-1} H_2O]
z_{i_s}	charge on surface species i_s
α	angle between flow direction and vertical axis
$\beta^e_{i_e,j_e}$	equivalent fraction of exchange species i_e on exchanger j_e (dimensionless)
$\beta^s_{i_s,j_s}$	mole fraction of surface species i_s on surface j_s
γ^m_j	activity coefficient for the jth aqueous master species (kg H_2O mol^{-1})
γ^x_y	activity coefficient for species y: x = l or e for aqueous or exchange species; $y = i_x$ is the index for the secondary species (kg H_2O mol^{-1})
λ	apparent thermal conductivity of the soil [M L T^{-3} K^{-1}]
θ	volumetric water content [L^3 L^{-3}]
$\nu^x_{y,z}$	stoichiometric coefficient of master species y in the reaction for secondary species z: superscripts x = l, e, s, p, and k are for aqueous species, exchange species, surface species, minerals, and kinetic reaction, respectively; subscripts $y = j_x$ is an index for the master species or kinetic reaction; $z = i_x$ is an index for the secondary species (dimensionless)
Ψ_{j_s}	surface potential for surface j_s [V]

Acknowledgments

This work was partly supported by the National Science Foundation, Agreement no. EAR-9876800 and the Terrestrial Sciences Program of the Army Research Office (Terrestrial Processes and Landscape Dynamics and Terrestrial System Modeling and Model Integration). Additional support was obtained through the bilateral agreement project "Development and evaluation of a coupled geochemical transport model" between SCK·CEN and USDA-ARS (Agreement no. 58-5310-0-F105), between SCK·CEN and the University of California, Riverside (Agreement no. C0-90001412.01), and by the SCK·CEN R&D Project CO91002.

References

Aagaard, P., and J.C. Helgeson. 1982. Thermodynamic and kinetic constraints on reaction rates among minerals and aqueous solutions: I. Theoretical considerations. Am. J. Sci. 282:237–285.

Appelo, C.A.J., and D. Postma. 2005. Geochemistry, groundwater, and pollution. 2nd ed. A.A. Balkema, Rotterdam, the Netherlands.

Appelo, C.A.J., E. Verweij, and H. Schäfer. 1998. A hydrogeochemical transport model for an oxidation experiment with pyrite/calcite/exchangers/organic matter containing sand. Appl. Geochem. 13:257–268.

Ball, J.W., and D.K. Nordstrom. 1991. WATEQ4F: User's manual with revised thermodynamic data base and test cases for calculating speciation of major, trace and redox elements in natural waters. Open-File Rep. 90-129. USGS, Denver, CO.

Barber, S.A. 1995. Soil nutrient bioavailability: A mechanistic approach. 2nd ed. John Wiley & Sons, New York.

Barišić, D., S. Lulić, and P. Miletić. 1992. Radium and uranium in phosphate fertilizers and their impact on the radioactivity of waters. Water Res. 26:607–611.

Barnett, M.O., P.M. Jardine, and S.C. Brooks. 2002. U(VI) adsorption to heterogeneous subsurface media: Application of a surface complexation model. Environ. Sci. Technol. 36:937–942.

Barnett, M.O., P.M. Jardine, S.C. Brooks, and H.M. Selim. 2000. Adsorption and transport of uranium(VI) in subsurface media. Soil Sci. Soc. Am. J. 64:908–917.

Berner, R.A., J.-L. Rao, S. Chang, R. O'Brien, and K. Keller. 1998. Seasonal variability of adsorption and exchange equilibria in soil waters. Aquat. Geochem. 4:273–290.

Bethke, C.M., and P.V. Brady. 2000. How the K_d approach undermines ground water cleanup. Ground Water 38:435–443.

Bradford, S.A., J. Šimůnek, M. Bettahar, M.Th. van Genuchten, and S.R. Yates. 2003. Modeling colloid attachment, straining, and exclusion in saturated porous media. Environ. Sci. Technol. 37:2242–2250.

Bradford, S.A., J. Šimůnek, M. Bettahar, M.Th. van Genuchten, and S.R. Yates. 2006. Significance of straining in colloid deposition: Evidence and implications. Water Resour. Res. 42:W12S26, doi:10.1029/2005WR004791.

Brady, N.C. 1990. The nature and properties of soils. 10th ed. Macmillan, New York.

Brantley, S. 2003. Reaction kinetics of primary rock-forming minerals under ambient conditions. p. 73–118. *In* J.I. Drever (ed.) Fresh water geochemistry, weathering, and soils. Treatise on geochemistry. Vol 5. Pergamon Press, Oxford, UK.

Brooks, R.H., and A.T. Corey. 1966. Properties of porous media affecting fluid flow. J. Irrig. Drain. Div. Am. Soc. Civ. Eng. 92:61–88.

Bruggenwert, M.G.M., and A. Kamphorst. 1982. Survey of experimental information on cation exchange in soil systems. p. 141–203. *In* G.H. Bolt (ed.) Soil chemistry: B. Physico-chemical models. Elsevier, Amsterdam.

Calba, H., Firdaus, P. Cazevieille, C. Thée, R. Poss, and B. Jaillard. 2004. The dynamics of protons, aluminium, and calcium in the rhizosphere of maize cultivated in tropical acid soils: Experimental study and modelling. Plant Soil 260:33–46.

Campbell, G.S. 1985. Soil physics with BASIC. Elsevier, Amsterdam.

Carrillo-González, R., J. Šimůnek, S. Sauvé, and D. Adriano. 2006. Mechanisms and pathways of trace elements in soils. Adv. Agron. 91:111–178.

Cogné, F. 1993. L'énergie nucléaire dans notre environnement radioactive: Principales données chiffreés. Rev. Gen. Nucl. 2:97–103.

Cunningham, J.A., and I. Mendoza-Sanchez. 2006. Equivalence of two models for biodegradation during contaminant transport in groundwater. Water Resour. Res. 42:W02416, doi:10.1029/2005WR004205.

Dang, Y.P., R.C. Dalal, D.G. Edwards, and K.G. Tiller. 1994. Kinetics of zinc desorption from Vertisols. Soil Sci. Soc. Am. J. 58:1392–1399.

Davis, J.A., D.E. Meece, M. Kohler, and G.P. Curtis. 2004a. Approaches to surface complexation modeling of uranium(VI) adsorption on aquifer sediments. Geochim. Cosmochim. Acta 68:3621–3641.

Davis, J.A., S.B. Yabusaki, C.I. Steefel, J.M. Zachara, G.P. Curtis, G.B. Redden, L.J. Criscenti, and B.D. Honeyman. 2004b. Assessing conceptual models for subsurface reactive transport of inorganic contaminants. EOS 85:449, 455.

de Mars, H., and G. Garritsen. 1997. Interrelationship between water quality and groundwater flow dynamics in a small wetland system along a sandy hill ridge. Hydrol. Processes 11:335–351.

de Mars, H., M.J. Wassen, and H. Olde Venterink. 1997. Flooding and groundwater dynamics in fens in eastern Poland. J. Veg. Sci. 8:319–328.

DeNovio, N.M., J.E. Saiers, and J.N. Ryan. 2004. Colloid movement in unsaturated porous media: Recent advances and future directions. Vadose Zone J. 3:338–351.

Dzombak, D.A., and F.M.M. Morel. 1990. Surface complexation modeling:

Hydrous ferric oxide. John Wiley & Sons, New York.
European Commission. 1999. Radiation protection 95: Reference levels for workplaces processing materials with enhanced levels of naturally occurring radionuclides. A guide to assist implementation of Title VII of the European Basic Safety Standards Directive (BSS) concerning natural radiation sources. Eur. Commission, Luxembourg.
Finke, P. 2006. Modelling the genesis of Luvisols in late Weichsel loess. p. 29–30. *In* A. Samouëlian and S. Cornu (ed.) Proc. Worksh. on Modelling of Pedogenesis, Nancy, France. 2–4 Oct. 2006. INRA, Orléans.
Freedman, V.L., D.H. Bacon, K.P. Saripalli, and P.D. Meyer. 2004. A film depositional model of permeability for mineral reactions in unsaturated media. Vadose Zone J. 3:1414–1424.
Gargiulo, G., S. Bradford, J. Šimůnek, P. Ustohal, H. Vereecken, and E. Klumpp. 2007. Bacterial transport and deposition under unsaturated conditions: The role of the matrix grain size and the bacteria surface protein. J. Contam. Hydrol. 92:255–273.
Geelhoed, J.S., W.H. Van Riemsdijk, and G.R. Findenegg. 1999. Simulation of the effect of citrate exudation from roots on the plant availability of phosphate adsorbed on goethite. Eur. J. Soil Sci. 50:379–390.
Goldberg, S., L.J. Criscenti, D.R. Turner, J.A. Davis, and K.J. Cantrell. 2007. Adsorption–desorption processes in subsurface reactive transport modeling. Vadose Zone J. 6:407–435.
Gonçalves, M.C., J. Šimůnek, T.B. Ramos, J.C. Martins, M.J. Neves, and F.P. Pires. 2006. Multicomponent solute transport in soil lysimeters irrigated with waters of different quality. Water Resour. Res. 42:W08401, doi:10.1029/2005WR004802.
Greskowiak, J., H. Prommer, G. Massmann, C.D. Johnston, G. Nützmann, and A. Pekdeger. 2005. The impact of variably saturated conditions on hydrogeochemical changes during artificial recharge of groundwater. Appl. Geochem. 20:1409–1426.
Guzman, E.T.T., M.V.E. Alberich, and E.O. Regil. 2002. Uranium and phosphate behavior in the vadose zone of a fertilized corn field. J. Radioanal. Nucl. Chem. 254:509–517.
Hopmans, J.W., and K.L. Bristow. 2002. Current capabilities and future needs of root water and nutrient uptake modelling. Adv. Agron. 77:103–183.
Jacques, D., and J. Šimůnek. 2005. User manual of the multicomponent variably saturated transport model HP1: Description, verification and examples. Version 1.0. BLG-998. SCK·CEN, Mol, Belgium.
Jacques, D., J. Šimůnek, D. Mallants, and M.Th. van Genuchten. 2006a. Modelling uranium leaching from agricultural soils to groundwater as a criterion for comparison with complementary safety indications. Mater. Res. Soc. Symp. Proc. 932:1057–1064.
Jacques, D., J. Šimůnek, D. Mallants, and M.Th. van Genuchten. 2006b. Operator-splitting errors in coupled reactive transport codes for transient variably saturated flow and contaminant transport in layered soil profiles. J. Contam. Hydrol. 88:197–218.
Jacques, D., J. Šimůnek, D. Mallants, and M.Th. van Genuchten. 2008. Modelling coupled water flow, solute transport and geochemical reactions affecting heavy metal migration in a podzol soil. Geoderma (in press), doi:10.1016/j.geoderma.2008.01.009.
Jansen, B., K.G.J. Nierop, and J.M. Verstraten. 2002. Influence of pH and metal/carbon ratios on soluble organic complexation of Fe(II), Fe(III) and Al in soil solutions determined by diffusive gradients in thin films. Anal. Chim. Acta 454:259–270.
Jin, Y., M.V. Yates, and S.R. Yates. 2002. Microbial transport. p. 1481–1509. *In* J.H. Dane and G.C. Topp (ed.) Methods of soil analysis. Part 4. Physical methods. SSSA Book Ser. 5. SSSA, Madison, WI.
Joris, I. 2005. Soil water dynamics in alluvial wetlands: Field and modelling study. Ph.D. diss. Univ. of Leuven, Leuven, Belgium.
Jury, W.A., and K. Roth. 1990. Transfer functions and solute movement through soil: Theory and applications. Birkhäuser, Berlin.
Kohler, M., G.P. Curtis, D.B. Kent, and J.A. Davis. 1996. Experimental investigation and modeling of uranium(VI) transport under variable chemical conditions. Water Resour. Res. 32:3539–3551.
Kuechler, R., and K. Noack. 2002. Transport of reacting solutes through the unsaturated zone. Transp. Porous Media 49:361–375.
Kuechler, R., and K. Noack. 2007. Comparison of the solution behaviour of a pyrite–calcite mixture in batch and unsaturated sand column. J. Contam. Hydrol. 90:203–220.
Langmuir, D. 1997. Aqueous environmental geochemistry. Prentice Hall, New Jersey.
Lasaga, A.C. 1981. Transition state theory. p. 169–195. *In* A.C. Lasaga et al. (ed.) Kinetics of geochemical process. Rev. Mineral. 8. Min. Soc. Am., Washington, DC.
Lasaga, A.C. 1995. Fundamental approaches in describing mineral dissolution and precipitation rates. p. 23–86. *In* A.F. White et al. (ed.) Chemical weathering rates of silicate minerals. Rev. Mineral. 31. Min. Soc. Am., Washington, DC.
Lasaga, A.C. 1998. Kinetic theory in the earth sciences. Princeton Univ. Press, Princeton, NJ.
Le Gallo, Y., O. Bildstein, and E. Brosse. 1998. Coupled reaction–flow modelling of diagenetic changes in reservoir permeability, porosity and mineral compositions. J. Hydrol. 209:366–388.
Lenhart, J.J., S.E. Cabaniss, P. MacCarthy, and B.D. Honeyman. 2000. Uranium(VI) complexation with citric, humic and fulvic acids. Radiochim. Acta 88:345–353.
Lenhart, J.J., and B.D. Honeyman. 1999. Uranium(VI) sorption to hematite in the presence of humic acid. Geochim. Cosmochim. Acta 63:2891–2901.
Lichtner, P.C. 1996. Continuum formulation of multicomponent–multiphase reactive transport. p. 1–81. *In* P.C. Lichtner et al. (ed.) Reactive transport in porous media. Rev. Mineral. 34. Min. Soc. Am., Washington, DC.
Lichtner, P.C., S. Yabusaki, K. Pruess, and C.I. Steefel. 2004. Role of competitive cation exchange on chromatographic displacement of cesium in the vadose zone beneath the Hanford S/SX tank farm. Vadose Zone J. 3:203–219.
Mayer, U. 1999. A numerical model for multicomponent reactive transport in variably saturated porous media. Ph.D. diss. Dep. of Earth Sciences, Univ. of Waterloo, Waterloo, ON, Canada.
Mayer, K.U., E.O. Frind, and D.W. Blowes. 2002. Multicomponent reactive transport modeling in variably saturated porous media using a generalized formulation for kinetically controlled reactions. Water Resour. Res. 38:1174, doi:10.1029/2001WR000862.
McKinley, J.P., J.M. Zachara, S.C. Smith, and G.D. Turner. 1995. The influence of uranyl hydrolysis and multiple site-binding reactions on adsorption of U(VI) to montmorillonite. Clays Clay Miner. 43:586–598.
Metz, V., W. Pfingsten, J. Lützenkirchen, and W. Schüssler. 2002. TrePro 2002: Modelling of coupled transport reaction processes. Worksh. of the Forschungszentrum Karlsruhe, 3rd, Karlsruhe, Germany. 20–21 Mar. 2002. Available at www.fzk.de/fzk/groups/ine/documents/internetdokument/id_040291.pdf (verified 20 Mar. 2008). Forschungszentrum Karlsruhe, Karlsruhe.
MIRA Team. 2004. Milieu: en natuurrapport Vlaanderen. Achtergronddocument 2004 Vermesting. Available at www.milieurapport.be (verified 17 Apr. 2008). Vlaamse Milieumaatschappij (Flemish Environment Agency), Mechelen, Belgium.
Morel, F., and J. Hering. 1993. Principles and applications of aquatic chemistry. John Wiley & Sons, New York.
Morrison, S.J., R.R. Spangler, and V.S. Tripathi. 1995. Adsorption of uranium(VI) on amorphous ferric oxyhydroxide at high concentrations of dissolved carbon(IV) and sulfur(VI). J. Contam. Hydrol. 17:333–346.
Nowack, B., K.U. Mayer, S.E. Oswald, W. Van Beinum, C.A.J. Appelo, D. Jacques, P. Seuntjens, F. Gérard, B. Jaillard, A. Schnepf, and T. Roose. 2006. Verification and intercomparison of reactive transport codes to describe root-uptake. Plant Soil 285:305–321.
Nuclear Regulatory Commission. 2006. Proc. Int. Conf. on Conceptual Model Dev. for Subsurface Reactive Transport Modeling of Inorganic Contaminants, Radionuclides, and Nutrients. NUREG/CP-0193. Available at www.nrc.gov/reading-rm/doc-collections/nuregs/conference/cp0193/cp0193.pdf (verified 17 Apr. 2008). Office of Nuclear Regulatory Research, U.S. Nuclear Regulatory Commission, Washington, DC.
Nützmann, G., P. Viotti, and P. Aagaard. 2005. Reactive transport in soil and groundwater: Processes and models. Springer-Verlag, Berlin, Germany.
Öztürk, H.S., and L. Özkan. 2004. Effects of evaporation and different flow regimes on solute distribution in soil. Transp. Porous Media 56:245–255.
Papastefanou, C., S. Stoulos, A. Iaonnidou, and M. Manolopoulou. 2006. The application of phosphogypsum in agriculture and the radiological impact. J. Environ. Radioact. 89:188–198.
Parkhurst, D.L., and C.A.J. Appelo. 1999. User's guide to PHREEQC (Version 2): A computer program for speciation, batch-reaction, one-dimensional transport, and inverse geochemical calculations. Water-Resour. Invest. Rep. 99-4259. USGS, Denver, CO.
Penmann, H.L. 1948. Natural evaporation from open water, bare soils and grass. Proc. R. Soc. London Ser. A 190:120–145.

Rockhold, M.L., R.R. Yarwood, M.R. Niemet, P.J. Bottomley, and J.S. Selker. 2002. Considerations for modeling bacterial-induced changes in hydraulic properties of variably saturated porous media. Adv. Water Resour. 25:477–495.

Rockhold, M.L., R.R. Yarwood, M.R. Niemet, P.J. Bottomley, and J.S. Selker. 2005. Experimental observations and numerical modeling of coupled microbial and transport processes in variably saturated sand. Vadose Zone J. 4:407–417.

Rockhold, M.L., R.R. Yarwood, and J.S. Selker. 2004. Coupled microbial and transport processes in soils. Vadose Zone J. 3:368–383.

Rothbaum, H.P., D.A. McGaveston, T. Wall, A.E. Johnston, and G.E.G. Mattingly. 1979. Uranium accumulation in soils from long-continued applications of superphosphate. J. Soil Sci. 30:147–153.

Saaltink, M.W., F. Battle, C. Ayora, J. Carrera, and S. Olivella. 2004. RETRASO, a code for reactive transport in saturated and unsaturated porous media. Geol. Acta 2:235–251.

Saito, H., J. Šimůnek, and B.-P. Mohanty. 2006. Numerical analysis of coupled water, vapor, and heat transport in the vadose zone. Vadose Zone J. 5:784–800.

Salvage, K.M., and G.T. Yeh. 1998. Development and application of a numerical model of kinetic and equilibrium microbiological and geochemical reactions (BIOKEMOD). J. Hydrol. 209:27–52.

Samper, J., R. Juncosa, J. Delgado, and L. Montenegro. 2000. CORE^{2D}: A code for nonisothermal water flow and reactive solute transport. User manual Version 2. Tech. Publ. 06/2000. Empresa Nacional de Residuos Radioactivos, Madrid.

Santos, A.J.G., B.P. Mazzilli, D.I.T. Favoro, and P.S.C. Silva. 2006. Partitioning of radionuclides and trace elements in phosphogypsum and its source materials based on sequential extraction methods. J. Environ. Radioact. 87:52–61.

Saripalli, K.P., V.L. Freedman, B.P. McGrail, and P.D. Meyer. 2006. Characterization of the specific solid–water interfacial area–water saturation relationship and its import to reactive transport. Vadose Zone J. 5:777–783.

Saueia, C.H.R., and B.P. Mazzilli. 2006. Distribution of natural radionuclides in the production and use of phosphate fertilizers in Brazil. J. Environ. Radioact. 89:229–239.

Schäfer, D., W. Schäfer, and W. Kinzelbach. 1998. Simulation of reactive processes related to biodegradation in aquifers. 1. Structure of the three-dimensional reactive transport model. J. Contam. Hydol. 31:167–186.

Seuntjens, P. 2000. Reactive solute transport in heterogeneous porous media: Cadmium leaching in acid sandy soils. Ph.D. diss. Univ. of Antwerp, Antwerp, Belgium.

Seuntjens, P., D. Mallants, N. Toride, C. Cornelis, and P. Geuzens. 2001a. Grid lysimeter study of steady-state chloride transport in two Spodosol types using TDR and wick samplers. J. Contam. Hydrol. 51:13–39.

Seuntjens, P., B. Nowack, and R. Schulin. 2005. Root-zone modeling of heavy metal uptake and leaching in the presence of organic ligands. Plant Soil 265:61–73.

Šimůnek, J., C. He, L. Pang, and S.A. Bradford. 2006. Colloid-facilitated solute transport in variably saturated porous media: Numerical model and experimental verification. Vadose Zone J. 5:1035–1047.

Šimůnek, J., N.J. Jarvis, M.Th. van Genuchten, and A. Gärdenäs. 2003. Review and comparison of models for describing non-equilibrium and preferential flow and transport in the vadose zone. J. Hydrol. 272:14–35.

Šimůnek, J., and D.L. Suarez. 1993. Modeling of carbon dioxide transport and production in soil: 1. Model development. Water Resour. Res. 29:487–497.

Šimůnek, J., and D.L. Suarez. 1994. Two-dimensional transport model for variably saturated porous media with major ion chemistry. Water Resour. Res. 30:1115–1133.

Šimůnek, J., and M.Th. van Genuchten. 2008. Modeling nonequilibrium flow and transport processes using HYDRUS. Vadose Zone J. 7:782–797 (this issue).

Šimůnek, J., M.Th. van Genuchten, and M. Šejna. 2005. The HYDRUS-1D software package for simulating the one-dimensional movement of water, heat, and multiple solutes in variably-saturated media. Version 3.0. HYDRUS Softw. Ser. 1. Dep. of Environmental Sciences, Univ. of California, Riverside.

Slattery, W.J., and G.R. Ronnfeldt. 1992. Seasonal variation of pH, aluminium and manganese in acid soils from north-eastern Victoria. Aust. J. Exp. Agric. 32:1105–1112.

Soler, J.M., and A.C. Lasaga. 1998. An advection–dispersion–reaction model of bauxite formation. J. Hydrol. 209:311–330.

Spalding, R.F., and W.M. Sackett. 1972. Uranium in runoff from the Gulf of Mexico distributive province: Anomalous concentrations. Science 175:629–631.

Steefel, C.I., D.J. DePaolo, and P.C. Lichtner. 2005. Reactive transport modeling: An essential tool and new research approach for the Earth sciences. Earth Planet. Sci. Lett. 240:539–558.

Stolk, A.P. 2001. Landelijk Meetnet Regenwatersamenstelling, Meetresultaten 1999. RIVM Rep. 723101056. Natl. Inst. for Public Health and the Environ. (RIVM), Bilthoven, the Netherlands.

Suarez, D.L., and J. Šimůnek. 1993. Modeling of carbon dioxide transport and production in soil: 2. Parameter selection, sensitivity analysis, and comparison of model predictions to field data. Water Resour. Res. 29:499–513.

Taylor, S.W., and P.R. Jaffé. 1990. Substrate and biomass transport in a porous medium. Water Resour. Res. 26:2181–2194.

Tebes-Stevens, C., A.J. Valocchi, J.M. VanBriesen, and B.E. Rittman. 1998. Multicomponent transport with coupled geochemical and microbiological reactions: Model description and example simulations. J. Hydrol. 209:8–26.

Tinker, P.B., and P.H. Nye. 2000. Solute movement in the rhizosphere. Oxford Univ. Press, New York.

Tipping, E. 2002. Cation binding by humic substances. Cambridge Univ. Press, Cambridge, UK.

van der Lee, J., and L. De Windt. 2001. Present state and future directions of modeling of geochemistry in hydrogeological systems. J. Contam. Hydrol. 47:265–282.

van der Lee, J., L. De Windt, V. Lagneau, and P. Goblet. 2003. Module-oriented modeling of reactive transport with HYTEC. Comput. Geosci. 29:265–275.

van Genuchten, M.Th. 1980. A closed-form equation for predicting the hydraulic conductivity of unsaturated soils. Soil Sci. Soc. Am. J. 44:892–898.

van Genuchten, M.Th. 1987. A numerical model for water and solute movement in and below the root zone. Res. Rep. 121. U.S. Salinity Lab., Riverside, CA.

van Genuchten, M.Th., and J. Šimůnek. 2004. Integrated modeling of vadose zone flow and transport processes. p. 37–69. *In* R.A. Feddes et al. (ed.) Unsaturated-zone modelling: Progress, challenges and applications. Frontis, Wageningen, the Netherlands.

Voegelin, A., V. Vulava, and R. Kretzschmar. 2001. Reaction-based model describing competitive sorption and transport of Cd, Zn, and Ni in an acidic soil. Environ. Sci. Technol. 35:1651–1657.

Waite, T.D., J.A. Davis, T.E. Payne, G.A. Waychunas, and N. Xu. 1994. Uranium(VI) adsorption to ferrihydrite: Application of a surface complexation model. Geochim. Cosmochim. Acta 58:5465–5478.

Wan, J.M., and T.K. Tokunaga. 1997. Film straining of colloids in unsaturated porous media: Conceptual model and experimental testing. Environ. Sci. Technol. 31:2413–2420.

Wan, J.M., and T.K. Tokunaga. 2002. Partitioning of clay colloids at air–water interfaces. J. Colloid Interface Sci. 247:54–61.

Yarwood, R.R., M.L. Rockhold, M.R. Niemet, J.S. Selker, and P.J. Bottomley. 2006. Impact of microbial growth on water flow and solute transport in unsaturated porous media. Water Resour. Res. 42:W10405, doi:10.1029/2005WR004550.

Yeh, G.-T., and H.-P. Cheng. 1999. 3DHYDROGEOCHEM: A 3-dimensional model of density-dependent subsurface flow and thermal multispecies–multicomponent hydrogeochemical transport. EPA/600/R-98/159. USEPA, Ada, OK.

Zhang, F., R. Zhang, and S. Kang. 2003. Estimating temperature effects on water flow in variably saturated soils using activation energy. Soil Sci. Soc. Am. J. 67:1327–1333.

Zhu, C. 2003. A case against K_d–based transport models: Natural attenuation at a mill tailings site. Comput. Geosci. 29:351–359.

Zielinski, R.A., S. Asher-Bolinder, A.L. Meier, C.A. Johnson, and B.J. Szabo. 1997. Natural or fertilizer-derived uranium in irrigation drainage: A case study in southeastern Colorado, U.S.A. Appl. Geochem. 12:9–21.